Journal of Molecular Graphics and Modelling 40 (2013) 1–9

Contents lists available at SciVerse ScienceDirect

Journal of Molecular Graphics and Modelling

journal homepage: www.elsevier.com/locate/JMGM

Elucidating the catalytic mechanism of β-secretase (BACE1): A quantum mechanics/molecular mechanics (QM/MM) approach

Arghya Barman, Rajeev Prabhakar*

Department of Chemistry, University of Miami, 1301 Memorial Drive, Coral Gables, FL 33146, United States

ARTICLE INFO

Article history:
Accepted 17 December 2012
Available online 5 January 2013

Keywords:
Alzheimer's disease
Aspartyl proteases
Beta-secretase
Protein hydrolysis
Acid-base mechanism

ABSTRACT

In this quantum mechanics/molecular mechanics (QM/MM) study, the mechanisms of the hydrolytic cleavage of the Met2-Asp3 and Leu2-Asp3 peptide bonds of the amyloid precursor protein (WT-substrate) and its Swedish mutant (SW) respectively catalyzed by β-secretase (BACE1) have been investigated by explicitly including the electrostatic and steric effects of the protein environment in the calculations. BACE1 catalyzes the rate-determining step in the generation of Alzheimer amyloid beta peptides and is widely acknowledged as a promising therapeutic target. The general acid-base mechanism followed by the enzyme proceeds through the following two steps: (1) formation of the gem-diol intermediate and (2) cleavage of the peptide bond. The formation of the gem-diol intermediate occurs with the barriers of 19.6 and 16.1 kcal/mol for the WT- and SW-substrate respectively. The QM/MM energetics predict that with the barriers of 21.9 and 17.2 kcal/mol for the WT- and SW-substrate respectively the cleavage of the peptide bond occurs in the rate-determining step. The computed barriers are in excellent agreement with the measured barrier of ~18.0 kcal/mol for the SW-substrate and in line with the experimental observation that the cleavage of this substrate is sixty times more efficient than the WT-substrate.

1. Introduction

Beta-secretase (BACE1) constitutes a family of aspartyl protease enzymes that is present in vertebrates, fungi, plants and retroviruses [1–4]. These enzymes are divided into the following two classes: (I) pepsin-like (renin, cathepsin D, chymosin, beta secretase, etc.) and (II) retroviral (HIV protease and malaria protease) [5,6]. BACE1 catalyzes the hydrolytic cleavage of a large number (~80) of proteins that are involved in several critical biological reactions [7,8]. One of the most notable functions of this enzyme is the catalysis of the rate-limiting step of Alzheimer amyloid beta (Aβ) peptide generation through the cleavage of the Met671-Asp672 amide bond of amyloid precursor protein (APP) (isoform 770, identifier –P05067) [9,10]. The Aβ peptides are the major components of plaques that are deposited in the brains of patients suffering from Alzheimer's disease (AD) [10–12]. A wealth of experimental data suggests that the inhibition of this enzyme is a very promising therapeutic target for the treatment of AD [9,10,13,14]. BACE1 knockout transgenic mice have been reported to be incapable of producing Aβ from either endogenous APP [15] or mutant APP transgene [16]. These animals were found to be normal in all other measures examined; giving encouragement that BACE1 inhibitors might prevent Aβ production without major side effects.

A large number of X-ray structures (ca. 170) of apo and inhibitor bound forms of this enzyme have been resolved [17–20]. These structures revealed that BACE1 consists of two main domains, namely the N-terminal domain and the C-terminal domain, and several specific sub-regions are distributed between them. The most critical regions of the enzyme known as 10s-loop (Lys9-Tyr14), flap (Val67-Glu77), insert-A (Gly158-Leu167), insert-D (Trp270-Thr274) and insert-F (Asp311-Asp317) facilitate the entry and binding of a substrate at the active site through their movements (Fig. 1) [17,21]. The active site of BACE1 contains a catalytic Asp dyad formed by two aspartate residues (Asp32 and Asp228) [17]. This dyad has been implicated in the catalytic functioning of the entire family of aspartyl proteases including pepsin, renin, cathepsin D and HIV protease [22–29]. The mutation of either one of these aspartate residues destroys the activity of BACE1 [30]. A number of theoretical calculations and recent X-ray and neutron diffraction data show that one of the Asp residues remains protonated and the second one unprotonated during the catalytic cycle [31–33]. BACE1 has also been reported to cleave a double mutant (Lys670 (P2) → Asn and Met671 (P1) → Leu) of APP known as the Swedish mutant (SW) sixty time more efficiently than the wild-type (WT)-substrate (P1, P2,. . .,consecutively denote the amino acid residues that flank the N-terminal of the substrate) (Fig. 2a) [34].

* Corresponding author. Tel.: +1 305 284 9372; fax: +1 305 284 4571.
E-mail address: rpr@miami.edu (R. Prabhakar).

1093-3263/$ – see front matter © 2013 Elsevier Inc. All rights reserved.
http://dx.doi.org/10.1016/j.jmgm.2012.12.010

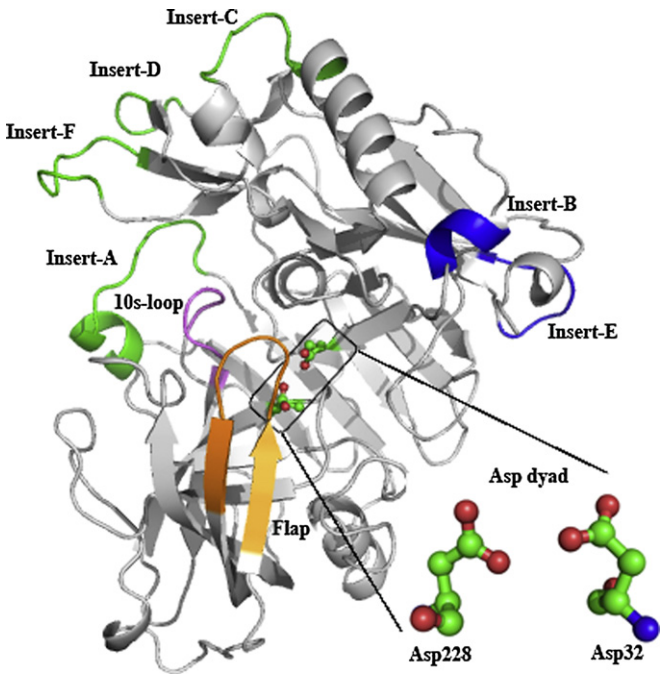

Fig. 1. Key regions of BACE1 from the X-ray structure (PDB ID: 1FKN).

BACE1 utilizes the general acid-base mechanism (discussed below) to cleave the peptide bond during its catalytic cycle [22]. This mechanism has previously been theoretically investigated for the other aspartyl proteases such as HIV protease [23–27] and presenilin (PS1) [28]. In addition, it has been studied by applying *ab initio* methods on simple models [35–37]. The most plausible mechanism of peptide hydrolysis has been proposed to proceed through the following two steps (Fig. 2b) [26,38]. In the first step, the unprotonated Asp228 acts as a base and the protonated Asp32 acts as an acid. From reactant (I), the Asp228 residue abstracts a proton from the catalytic water molecule (W1) and generates a hydroxyl ion (OH^-). The generated hydroxyl ion subsequently makes a nucleophilic attack on the carbonyl carbon of the scissile peptide bond and concomitantly the Asp32 donates its proton to the carbonyl oxygen of the peptide bond to produce the tetrahedral gem-diol intermediate (II). From (II), the two aspartates reverse their functions and Asp32 now acts as a base and Asp228 acts as an acid. The protonated Asp228 donates its proton to the amide nitrogen (—NH) of the scissile peptide bond and in a synchronous manner Asp32 abstracts a proton from one of the hydroxyl groups (—OH) of the gem-diol intermediate. This process leads to the cleavage of the peptide bond that generates the amino ($—NH_2$) and carboxy (—COOH) terminals (III). Experimentally measured kinetic data ($k_{cat} = 2.45\ s^{-1}$) for the SW-substrate shows that the reaction proceeds through a barrier of ca. 18.0 kcal/mol [34]. In a QM/MM study, Carloni et al. also showed that the formation of the gem-diol species (first step) for the Leu-Ala substrate peptide occurs through a barrier of ca. 20.0 kcal/mol [25]. In this study, only the first step of the mechanism was investigated and the barrier was estimated by keeping the distance between the oxygen atom of the catalytic water and the carbon atom of the peptide bond of the substrate fixed at increasingly shorter distances. In a previous QM only (DFT) study using a pruned model of the active site, with the barrier of 22.4 and 19.1 kcal/mol for the WT- and SW-substrate respectively, this step was proposed to be the rate-determining step for both substrates [29]. However, a Car-Parrinello MD simulation study on another member of the aspartyl protease family, HIV protease, suggested that the peptide bond cleavage in the second step (barrier = 21.0 kcal/mol) occurs in the rate-determining step [26]. Here, the barriers for both steps were estimated by constraining the reaction coordinates. The main conclusion of this study was also supported by a recent crystallographic study on HIV protease [39].

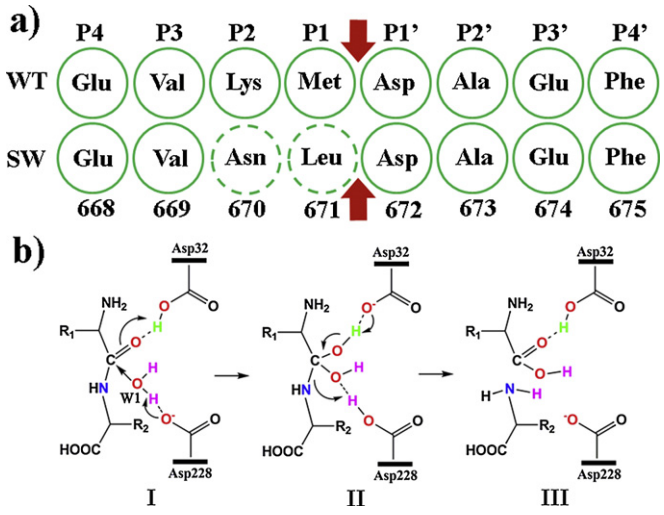

Fig. 2. (a) Amino acid sequences of the WT- and SW substrates. The mutated residues in the SW substrate are marked as dotted circles and the arrow signs show the cleavage site of the substrates. (b) General acid/base mechanism utilized by BACE1.

In almost all the previous studies, either the pruned models of the active sites have been utilized or key reaction coordinates were constrained to investigate catalytic mechanisms. In calculations using these models the electrostatic and steric effects of the protein environment surrounding the active site were either completely ignored or only the latter was partially included by constraining some atoms from the X-ray structures. Therefore, these studies cannot incorporate the influence of these effects on the computed energetics and elucidate the reorganization of the key regions (the 10s-loop, flap, insert-A, insert-D and insert-F) of the enzyme in each step of the reaction.

In order to address these outstanding issues, we have employed a hybrid two-layer quantum mechanics/molecular mechanics (QM/MM) method, ONIOM (B3LYP/Amber), to investigate the mechanisms of the hydrolysis of WT- and SW-substrate by including the entire enzyme in the models. The fully optimized structures derived from these calculations will provide the quantitative contribution of the electrostatic and steric effects of the protein on energetics and the structural changes in the key regions of the enzymes during the mechanism. The structural and mechanistic information revealed by these calculations will also help to understand the cleavage mechanisms of different biological substrates (~80) of this critical enzyme and other members of the aspartyl protease family.

2. Computational models

The starting structures of the enzyme-substrate (BACE1-WT and BACE-SW) complexes are obtained from our previous MD simulations [29]. The models used in this study include all 393 amino acid residues of the enzyme and octa-peptide substrate. The BACE-WT and BACE-SW complexes contain 6101 and 6095 atoms respectively in total and the whole enzyme-substrate complex is called the "real" system. The "model (QM)" part of the "real" system includes six residues (Asp32, Ser35, Tyr71, Asp228, Thr231 and Arg235) from the enzyme and four from the substrate (Lys1, Met2, Asp3 and Ala4 of the WT-substrate and Asn1, Leu2, Asp3 and Ala4 residues of the SW-substrate) and two water molecules (W1 and

W2). The model part contains 161 and 155 atoms in total for the BACE1-WT and BACE1-SW complexes respectively. The charge states of this part for BACE1-WT and BACE1-SW are 0 and −1 respectively.

3. Computational procedure

All calculations were performed utilizing the Gaussian 09 (G09) program [40]. The ONIOM calculations were performed using the two-layer ONIOM (QM/MM) method [41–46]. The atoms linking the QM (model) and MM (real) parts were treated as hydrogen atoms [47,48]. The interaction between the QM and MM regions was computed using the mechanical embedding scheme [41–45]. The total energy of the system is calculated utilizing the following equation:

$$E_{\mathrm{ONIOM}} = E_{\mathrm{MM,real}} + E_{\mathrm{QM,model}} - E_{\mathrm{MM,model}}$$

In this equation $E_{\mathrm{MM,real}}$, $E_{\mathrm{QM,model}}$ and $E_{\mathrm{MM,model}}$ denotes the MM energy of the "real" system, the QM energy of the "model" system and the MM energy of the "model" system respectively. The effect of the protein surrounding is evaluated as: $\Delta E_{\mathrm{MM}} = \Delta E_{\mathrm{MM,real}} - \Delta E_{\mathrm{MM,model}}$. In this study, the "model" part is treated at the B3LYP level using the all-electron 6-31G(d) basis set as implemented in G09 [49–51]. The "real" system was treated at the MM level utilizing the AMBER force field [52].

All degrees of freedom were optimized and each transition state was confirmed to have a single imaginary frequency corresponds to the reaction coordinate. The final energetics of the optimized structures were improved by including the single point energy from the triple zeta quality of basis set (6-311+G(d,p)), unscaled zero-point energy and thermal correction (at 298.15 K and 1 atm) estimated at the B3LYP/6-31G(d) level using the "active site only" model from our previous study [29].

Due to the iterative nature of the QM/MM methods, in some cases the changes in the conformational space (MM part) might not be connected with the actual reaction coordinates in the QM part. Therefore, to compare energies of different minima and saddle points on the potential energy surface (PES), the corresponding transition state and minima were localized, back and forth, to confirm that these structures are connected with each other. To ascertain that the reaction proceeding in the same conformational space, the root-mean-square-deviations (rmsd) of the "real" part (including hydrogen atoms) of every single structure were also compared with the previous one. Furthermore, the MM atom types of the atoms belong to reaction coordinates formally change during the reaction. Thus, the effects (0.3–0.5 kcal/mol) of the changes in the MM parameters were also included in the final energies. The ONIOM method has previously been successfully employed to study the mechanisms of several important enzymes such as methane monooxygenase, ribonucleotide reductase, methylmalonyl-CoA mutase, isopenicillin n-synthase and glutathione peroxidase [53–60].

4. Results and discussion

In the present QM/MM study, the mechanisms for the hydrolysis of Met2-Asp3 and Leu2-Asp3 peptide bonds of the WT-and SW-substrate respectively catalyzed by BACE1 have been investigated by including the entire enzyme in the models. In the next section, first the structures, mechanism and energetics of the hydrolysis of the WT-substrate will be discussed followed by their comparisons with the case of the SW-substrate.

Table 1
The root-mean-square deviation (in Å) of the WT-BACE1 and SW-BACE1 complexes relative to the corresponding reactants.

	WT		SW	
	Real (Å)	Model (Å)	Real (Å)	Model (Å)
I → TSI	0.13	0.35	0.07	0.24
I → II	0.13	0.37	0.07	0.26
I → TSII	0.61	0.65	0.12	0.39
I → III	0.67	0.60	0.09	0.35

4.1. Hydrolysis of the WT- substrate

4.1.1. Formation of the gem-diol intermediate

In the optimized reactant for the WT-substrate (I_{WT}), a water molecule (W1, H_2O^3) interacts with the Asp32 (protonated) and Asp228 (unprotonated) residues of the catalytic Asp dyad through hydrogen bonds ($O^3H{-}O^7$ = 2.33 Å and $O^3H{-}O^2$ = 1.47 Å) (Fig. 3). The side chain (O^1H) of Asp32 is observed to make a hydrogen bond with the carbonyl oxygen of Met2 of the substrate ($O^1H{-}O^4$ = 1.77 Å). In I_{WT}, the catalytic dyad (Asp32-Asp228) is involved in a hydrogen bonding network with the neighboring residues Ser35, Tyr71, Thr231 and another water molecule (W2). The 10s-loop, flap, insert-A, insert-D and insert-F regions of the enzyme interact with each other and position the substrate in a bio-active conformation for the hydrolysis. In I_{WT}, the 10s-loop interacts with the insert-F through a hydrogen bond between the Lys9 and Glu310 residues of these regions respectively (Fig. S1a). This interaction moves the insert-F closer to the active site and its Asp311 makes a strong hydrogen bond with the N-terminal of the substrate. It also interacts with the insert-D through the Asp317 (insert-F) – Gln271 (insert-D) bond. The side chain of Gln73 of the flap also forms a strong hydrogen bond with the side chain of Lys1 of the substrate (Fig. S2). The total volume of the enzyme cavity calculated using the pocket-finder server in I_{WT} is 800 Å^3.

In the first step of this reaction, the protonated Asp32 and unprotonated Asp228 act as an acid and base respectively. From I_{WT}, Asp228 activates the W1 (H_2O^3) water molecule by abstracting a proton and generates the hydroxyl nucleophile (O^3H^-). The $-O^3H$ ion attacks the C^5 atom of the scissile peptide bond ($C^5{-}N^6$) concomitantly with the donation of a proton from Asp32 to the carbonyl group ($C^5{=}O^4$) of the bond. The fully optimized transition state structure (TSI_{WT}) is shown in Fig. 3. In TSI_{WT}, all the relevant bond distances ($O^2{-}H$ = 1.11 Å, $O^3{-}H$ = 1.35 Å, $O^3{-}C^5$ = 1.74 Å, $O^1{-}H$ = 1.41 Å and $O^4{-}H$ = 1.08 Å) indicate that this process is synchronous. The barrier of 19.6 kcal/mol for this step is in excellent agreement with the experimentally measured barrier of ∼18.0 kcal/mol [34]. In the $I_{WT} \rightarrow TSI_{WT}$ process, the active site of the enzyme undergoes noticeable reorganization (rmsd = 0.35 Å) and Asp228 and Thr231 of BACE1 and Lys1, Met2 and Asp3 of the substrate were found to be the most dynamic (rmsd > 0.50 Å) (Fig. 4a and Table 1). However, this step does not cause long range structural changes in the enzyme, which retains its overall structure (rmsd = 0.13 Å). Furthermore, structures of the key regions largely remain unchanged and they exhibit small rmsd from I_{WT} i.e. 10s-loop (0.09 Å), flap (0.14 Å), insert-A (0.07 Å), insert-D (0.06 Å) and insert-F (0.09 Å).

This step leads to the creation of a tetrahedral gem-diol intermediate (II_{WT}) in which two hydroxyl groups ($-O^3H$ and $-O^4H$) are attached to the C^5 atom of the peptide bond. The formation of II_{WT} is endothermic by 14.7 kcal/mol (Table 2). II_{WT} is stabilized by the hydrogen bonding network created by the interaction of $C^5{-}O^4H$ and $C^5{-}O^3H$ groups with the O^1 and O^7 respectively from Asp32 ($O^1{-}O^4H$ = 1.76 Å and $O^7{-}O^3H$ = 1.67 Å). In addition, the $-O^2H$ group of Asp228 forms a strong hydrogen bond with

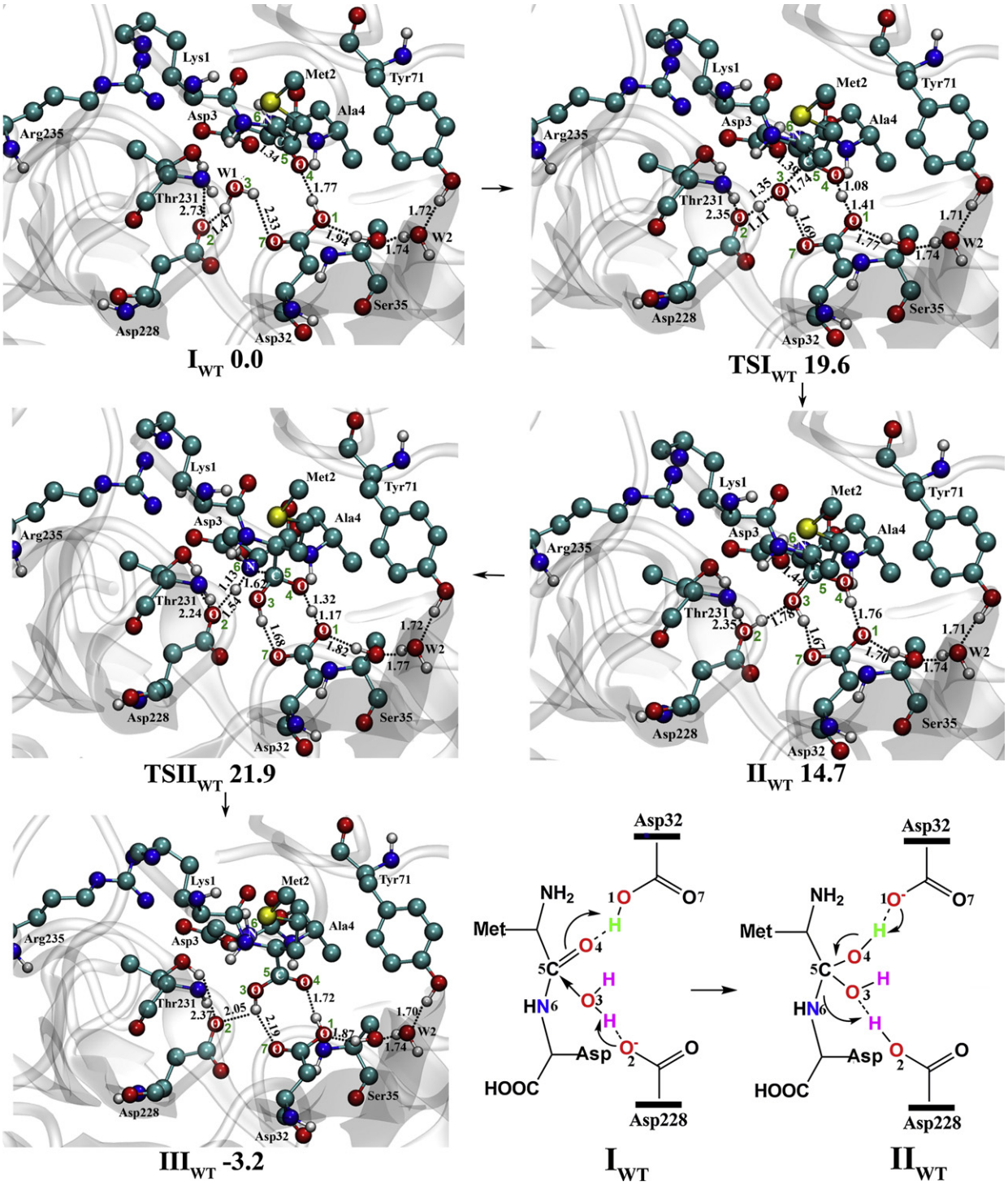

Fig. 3. Structures (in Å) and energies (in kcal/mol) of the optimized reactant, intermediate, transition states and product for the cleavage of the Met2-Asp3 peptide bond of the WT substrate. The QM and MM parts are presented in ball and stick and cartoon models, respectively. The noncritical hydrogen atoms are omitted from the figure for clarity.

the O^3 atom ($O^2H{-}O^3$ = 1.78 Å). In other members of this family of enzymes (PS1 and HIV protease), the formation of this intermediate was also computed to be endothermic by more than 10.0 kcal/mol. The creation of the oxyanion species [$C(OH)(O^-)$] in this step was observed to be prohibitively high (>35.0 kcal/mol) for both PS1 [28] and HIV protease [61] and thus this possibility is not considered in this study. Since TSI_{WT} is located close to II_{WT} on PES, there are very small changes in the overall structure of the enzyme in this transition (rmsd = 0.13 Å) (Table 1). In addition, the overall conformations of the 10s-loop (0.09 Å), flap (0.13 Å), insert-A (0.06 Å), insert-D (0.07 Å) and insert-F (0.09 Å) remain unchanged.

4.1.2. Cleavage of the Met-Asp peptide bond

In this step, the constituents of the Asp dyad interchange their roles and Asp32 now acts as a base and Asp228 as an acid. From II_{WT}, Asp228 transfers the previously acquired proton to the N^6—H group of the Met2-Asp3 peptide bond. This process occurs with a simultaneous abstraction of the proton from the O^4 atom of

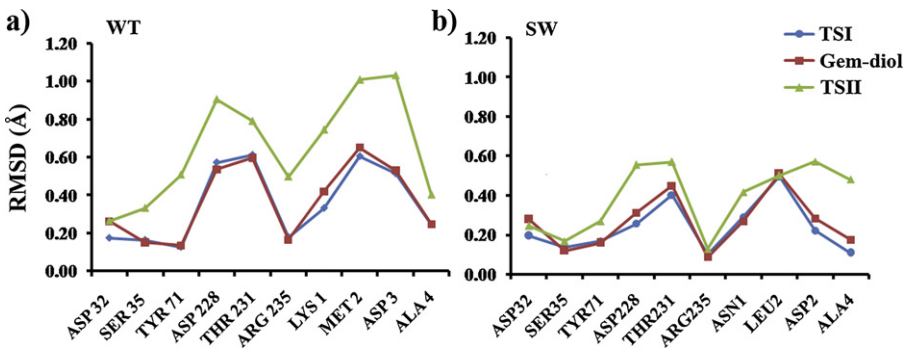

Fig. 4. Root-mean-square deviation (in Å) of the individual amino acid residues in the QM part of (a) BACE1-WT and (b) BACE1-SW complexes from their corresponding reactants.

the gem-diol intermediate by Asp32. This double proton transfer causes the cleavage of the scissile peptide bond (C^5—N^6) and the fully optimized state ($TSII_{WT}$) for this process is shown in Fig. 3. In $TSII_{WT}$, all key bond distances (O^2—H = 1.54 Å, N^6—H = 1.13 Å, C^5—N^6 = 1.62 Å, O^4—H = 1.32 Å and O^1—H = 1.17 Å) indicate that this process is concerted. From II_{WT}, this process occurs with a barrier of 7.2 kcal/mol. Since this step is followed by a step that is endothermic by 14.7 kcal/mol the overall barrier for this process becomes 21.9 kcal/mol from I_{WT} (Table 2). This barrier is also in accord with the experimentally measured barrier of ~18.0 kcal/mol [34]. In contrast to the QM energetics [29], the inclusion of the electrostatic and steric effects of the enzyme increases the barrier for this step by 4.8 kcal/mol. In a recent crystallographic study [39] and Car-Parrinello MD simulations on HIV protease [26] this process was also suggested to take place in the rate-determining step.

In comparison to the previous step, this step introduces significant changes in both the active site and overall structure of the enzyme. The rmsd of the active site and enzyme are increased by 0.48 and 0.28 Å to 0.61 and 0.65 Å respectively from I_{WT} (Table 1). In particular, the Tyr71, Asp228, Thr231 and Arg235 residues of BACE1 and Lys1, Met2, and Asp3 of the substrate undergo large structural changes (Fig. 4a). These structural changes influence the structures of the other key regions of the enzyme. In comparison to I_{WT}, the 10s-loop, insert-A, insert-D and insert-F exhibit rmsds of 0.23, 0.43, 0.64 and 0.24 Å, respectively. However, the interaction between the 10s-loop and insert-F remains intact. The Gln73 and Gly74 residues of the flap undergo conformational changes and alter the enzyme's structure (rmsd = 0.85 Å). The Gln73(BACE1)-Lys1(substrate) hydrogen bond observed in I_{WT} is broken and Gln73 reorients itself to form a bond with the backbone 'O' of Glu (P4) of the substrate (Fig. S2). These changes push the Cα atoms of Gln73 and Gly74 away by 1.4 and 2.0 Å respectively from the corresponding positions in II_{WT}. In comparison to I_{WT}, the reorganization in the structure of the enzyme causes a significant reduction (70 $Å^3$) in the volume of the cavity in $TSII_{WT}$. This reduction indicates the stabilization of $TSII_{WT}$ by the enzyme in the step. The hydrolytic cleavage of the Met-Asp peptide bond leads to the generation of the separated Met-COOH and NH_2-Asp products (III_{WT}). The formation of III_{WT} is exothermic by 3.2 kcal/mol from I_{WT}.

These results show that the cleavage of the peptide bond occurs with 2.4 kcal/mol higher barrier than the one computed for the formation of the gem-diol intermediate. Although the barriers for both steps are in excellent agreement with the measured value of 18.0 kcal/mol, due to the accuracy of the computational method it is not possible to predict the rate-determining step in the mechanism.

Table 2
Calculated QM/MM energies for the reactants, transition states, intermediates, and products.

Transition	Energy (kcal/mol)
WT-substrate	ONIOM
$I_{WT} \rightarrow TSI_{WT}$	19.6
$I_{WT} \rightarrow II_{WT}$	14.7
$I_{WT} \rightarrow TSII_{WT}$	21.9
$I_{WT} \rightarrow III_{WT}$	−3.2
SW-substrate	
$I_{SW} \rightarrow TSI_{SW}$	16.1
$I_{SW} \rightarrow II_{SW}$	10.0
$I_{SW} \rightarrow TSII_{SW}$	17.2
$I_{SW} \rightarrow III_{SW}$	−1.6

4.2. Hydrolysis of the SW-substrate

4.2.1. Formation of the gem-diol intermediate

In the optimized reactant (I_{SW}) for the SW-substrate, the catalytic water W1 (H_2O^3) interacts with the Asp dyad through hydrogen bonds (O^3H—O^7 = 2.07 Å and O^3H—O^2 = 1.63 Å) (Fig. 5). In I_{SW}, the O^1—H of Asp32 makes a hydrogen bond with the carbonyl oxygen of Leu2 of the substrate (O^1H—O^4 = 1.80 Å). Similar to I_{WT}, both Asp32 and Asp228 residues are involved in a network of hydrogen bonds with the surrounding residues (Ser35, Tyr71, Thr231 and W2) in I_{SW}. The rmsd difference of 1.54 Å between I_{SW} and I_{WT} indicates substantial differences between these structures. In particular, the active site, 10s-loop, flap, insert-A, insert-D and insert-F regions undergo noticeable structural changes (Table S1 and Fig. S3). In the active site, the backbone 'NH' of Thr231 is found to interact with the O^2 of Asp228, whereas this interaction is completely lost in I_{WT}. In I_{SW}, the total volume of the cavity (830 $Å^3$) is greater than that computed for I_{WT} (800 $Å^3$). The protein surrounding the active site was found to play an important role in stabilizing the enzyme-substrate complex. In I_{SW}, the catalytic triad (Asp32-W1-Asp228) shifts toward the scissile peptide bond (C^5—N^6) and the distance between W1 and C^5 is 0.40 Å shorter than the one in I_{WT}.

From I_{SW}, similar to the WT-substrate case, the activation of the catalytic water (W1, H_2O^3) by the unprotonated Asp228 generates the hydroxyl ion (—O^3H^-) nucleophile that concomitantly attacks the carbonyl carbon (C^5) of the peptide bond (Fig. 5). This process is accompanied by simultaneous delivery of a proton from the Asp32 to the O^4 atom of the (C^5=O^4) group of the amide bond. In the optimized transition state structure (TSI_{SW} in Fig. 5), all the critical bond distances suggest that this process is concerted (O^2—H = 1.08 Å, O^3—H = 1.34 Å, O^3—C^5 = 1.75 Å, O^1—H = 1.33 Å and O^4—H = 1.07 Å). The computed barrier of 16.1 kcal/mol for this step is 3.5 kcal/mol lower than that of the WT-substrate. The reason for this reduction is likely to be the differences in key bond distances in TSI_{SW} and TSI_{WT}. In TSI_{SW}, in comparison to TSI_{WT}, the O^2—H, O^3 – H, O^1—H and O^4—H bond distances are shortened by 0.03, 0.01,

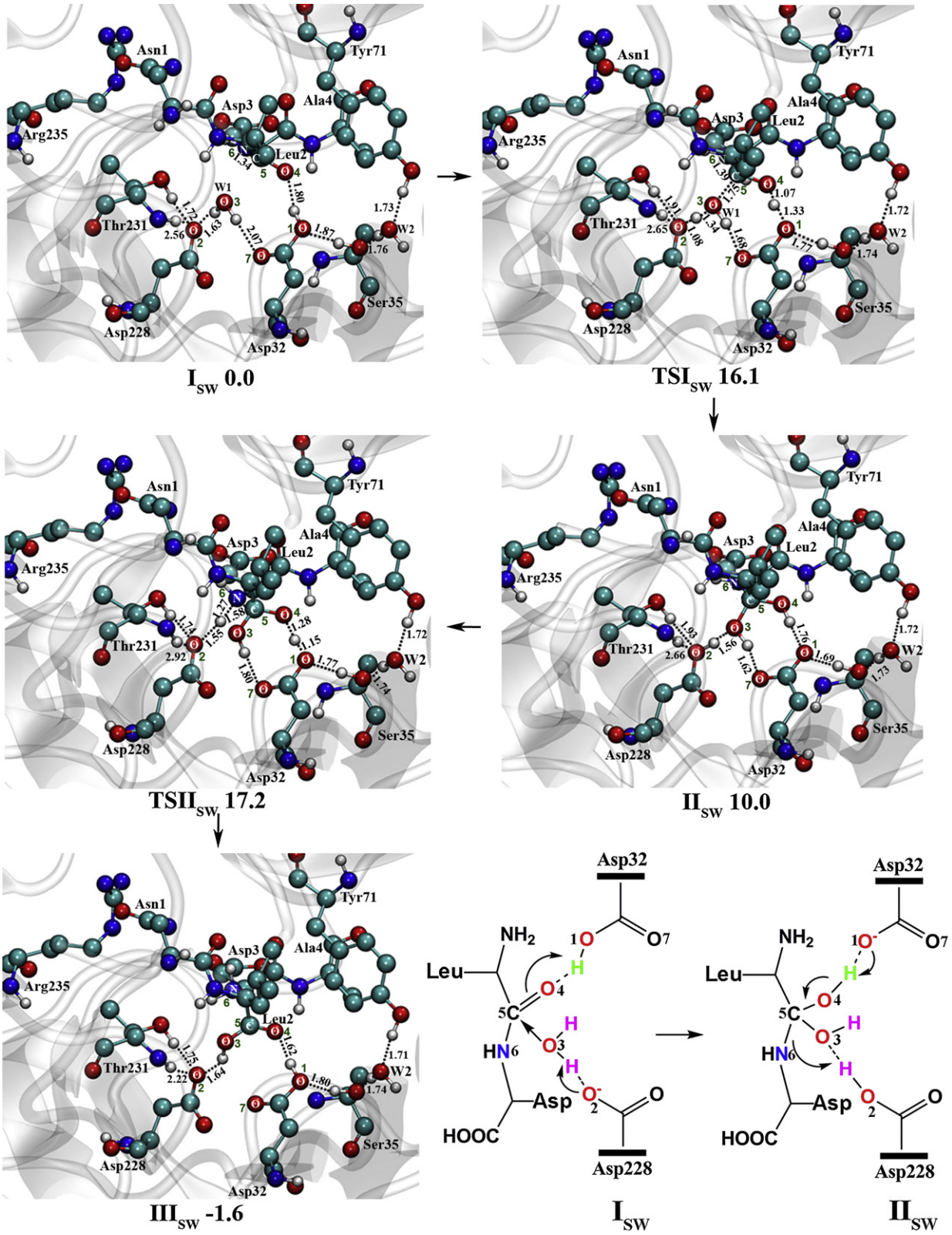

Fig. 5. Structures (in Å) and energies (in kcal/mol) of the optimized reactant, intermediate, transition states and product for the cleavage of the Leu2-Asp3 peptide bond of the SW substrate. The QM and MM parts are presented in ball and stick and cartoon models, respectively. The noncritical hydrogen atoms are omitted from the figure for clarity.

0.08 and 0.01 Å respectively, while the O^3—C^5 bond is elongated by 0.01 Å.

As observed in the BACE1-WT case, the enzyme retains its overall structure (rmsd = 0.07 Å) in the $I_{SW} \rightarrow TSI_{SW}$ process and only the active site undergoes moderate changes (rmsd = 0.24 Å) along the reaction coordinates (Table 1). At the active site, Thr231 of BACE1 and Leu2 of the substrate exhibit noticeable changes (rmsd > 0.40 Å) (Fig. 4b). Furthermore, the 10s-loop (rmsd = 0.11 Å)

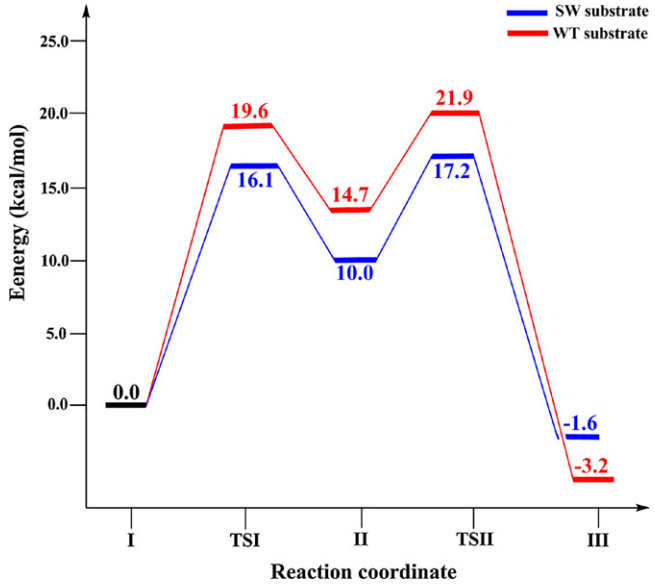

Fig. 6. Potential energy diagrams for the cleavage of the Met2-Asp3 peptide bond of the WT substrate (red line) and Leu2-Asp3 peptide bond of the SW substrate (blue line) catalyzed by BACE1.

and flap (rmsd = 0.16 Å) exhibit minor structural modifications, while insert-A (rmsd = 0.04 Å), insert-D (rmsd = 0.03 Å) and insert-F (rmsd = 0.03 Å) retain their stable conformations. Here, in addition to the Lys9 (10s-loop)-Glu310 (insert-F) bond that was also observed in the BACE1-WT case, two more hydrogen bonds Gln12 (10s-loop)-Glu310 (insert-F) and Asn162 (insert-A)-Glu310 (insert-F) are formed (Fig. S1b).

This step leads to the formation of the gem-diol intermediate (II_{SW}) that is 10.0 kcal/mol endothermic from I_{SW}. This intermediate is stabilized by a network of hydrogen bonds formed by Asp32 ($O^4H—O^1$ = 1.76 Å and $O^3H—O^7$ = 1.62 Å) and Asp228 ($O^2H—O^3$ = 1.56 Å). The endothermicity for the creation of II_{SW} is 4.7 kcal/mol lower than the one computed for II_{WT} (Table 2). The calculated rmsd values indicate that there are only small changes in the active site (rmsd = 0.26 Å), enzyme (rmsd = 0.07 Å), 10s-loop (rmsd = 0.11 Å), flap (rmsd = 0.14 Å), insert-A (rmsd = 0.04 Å), insert-D (rmsd = 0.04 Å) and insert-F (rmsd = 0.03 Å) in this process.

4.2.2. Cleavage of the Leu-Asp peptide bond

In this step, from II_{SW} Asp228 donates a proton to the $N^6—H$ group of the $C^5—N^6$ peptide bond and Asp32 simultaneously accepts the $O^4—H$ proton. This process leads to cleavage of the Leu2-Asp3 bond and produces the separated carboxyl ($—C^5O^4O^3H$) and amine ($—N^6H_2$) terminals. In the optimized transition state ($TSII_{SW}$ in Fig. 5), all the key distances show that this process is synchronous ($O^2—H$ = 1.55 Å, $N^6—H$ = 1.27 Å, $C^5—N^6$ = 1.58 Å, $O^4—H$ = 1.28 Å and $O^1—H$ = 1.15 Å). From II_{SW}, the barrier for this process is 7.2 kcal/mol i.e. 17.2 kcal/mol from the I_{SW} reactant. Similar to the energetics of the WT-substrate, the barrier for this step is slightly (1.1 kcal/mol) higher than the one computed in the first step. However, the barrier here is 4.7 kcal/mol lower than the one computed for the WT-substrate. The computed energetics is in accord with the experimental observation that the cleavage of the SW-substrate is sixty times more efficient than the WT-substrate [34]. Compared to $TSII_{WT}$, the $O^2—H$ and $N^6—H$ distances in $TSII_{SW}$ are increased by 0.01 and 0.14 Å respectively, whereas $O^4—H$, $C^5—N^6$and $O^1—H$ are shortened by 0.04, 0.04 and 0.02 Å, respectively.

As observed in the $II_{WT} \rightarrow TSII_{WT}$ transition, this process is also accompanied by significant structural changes in the active site and whole enzyme. Here the rmsd of the active site for this transition is increased by 0.13–0.39 Å from I_{SW} (Table 1). In particular, the Asp228 and Thr231 residues of BACE1 and Asn1, Asp3 and Ala4 of the substrate exhibit high deviations from II_{SW}. However, they are much less than the deviations observed in $TSII_{WT}$ (Fig. 4b). On the other hand, the overall structure of the enzyme (rmsd = 0.12 Å), the 10s-loop (rmsd = 0.14 Å), flap (rmsd = 0.23 Å), insert-F (rmsd = 0.12 Å), insert-A (rmsd = 0.07 Å) and insert-D (rmsd = 0.06 Å) show only small structural changes. In comparison to I_{SW} the volume of the enzyme cavity in $TSII_{SW}$ is also substantially reduced by 60 $Å^3$. The hydrolysis of the Leu2-Asp2 peptide bond creates the separated Leu-COOH and NH_2-Asp termini (III_{SW}). The formation of III_{SW} is only 1.6 kcal/mol exothermic from I_{SW}. In III_{SW}, the low rmsd values of the 10s-loop (0.09 Å), flap (0.22 Å), insert-A (0.04 Å), insert-D (0.09 Å) and insert-F (0.11 Å) indicate structural stability of $TSII_{SW}$ in this transition.

These results predict that, similar to the WT-substrate case, the barrier for the cleavage of the peptide bond is slightly higher (1.1 kcal/mol) for the SW-substrate and it is more efficient substrate of BACE1.

5. Summary and conclusions

In the present QM/MM (ONIOM:B3LYP/Amber) study, the catalytic mechanisms of the hydrolytic cleavage of the Met2-Asp3 and Leu2-Asp3 peptide bonds of the WT-and SW-substrate respectively by BACE1 have been investigated. The potential energy surface (PES) diagrams for these reactions are shown in Fig. 6. The formation of the gem-diol intermediate in the first step occurs with the barriers of 19.6 and 16.1 kcal/mol for the WT- and SW-substrate respectively. The creation of the gem-diol intermediate in this step for the SW-substrate (10.0 kcal/mol) is 4.7 kcal/mol more favorable than for the WT-substrate (14.7 kcal/mol).

The cleavage of the peptide bond of the WT-substrate occurs through a barrier of 21.9 kcal/mol, which is in good agreement with the experimentally measured barrier of ~18.0 kcal/mol [34]. For the SW-substrate, the barrier for this process is lower by 4.7 kcal/mol from I_{WT} i.e. 17.2 kcal/mol from the reactant I_{SW}. The decrease in the barrier for this substrate qualitatively supports the experimental observation that its cleavage is sixty times more efficient than the WT-substrate [15,34]. In this step, from I_{WT} and I_{SW} the significant structural modifications in the enzyme shrink its active site cavity by 60–70 $Å^3$ in the corresponding transition states ($TSII_{WT}$ and $TSII_{SW}$). In both cases the barrier for this step was found to be higher than the previous one. Although the QM/MM optimizations performed in this study provided accurate energetics of the reaction, the prediction of the free-energy can be further improved by the application of the recently developed orthogonal space random walk method [62].

The computed QM/MM energetics explicitly indicate that BACE1 is more efficient in cleaving the SW substrate compared to the WT substrate. The results presented in this study will enhance our understanding of the substrate specificity and cleavage mechanism of this critical enzyme and other aspartyl proteases.

Acknowledgements

A funding grant (DOH grant number 08KN-11) to R.P. from the James and Esther King Biomedical Research Program of the Florida State Health Department is acknowledged. Computational resources from the Center for Computational Science (CCS) at the University of Miami are greatly appreciated. We thank Erica Sturm for her assistance in the preparation of the manuscript.

Appendix A. Supplementary data

Supplementary data associated with this article can be found, in the online version, at http://dx.doi.org/10.1016/j.jmgm.2012.12.010.

References

[1] D.B. Northrop, Follow the protons: a low-barrier hydrogen bond unifies the mechanisms of the aspartic proteases, Accounts of Chemical Research 34 (2001) 790–797.
[2] D.R. Davies, The structure and function of the aspartic proteinases, Annual Review of Biophysics and Bioengineering 19 (1990) 189–215.
[3] M. Miller, M. Jaskolski, J.K.M. Rao, J. Leis, A. Wlodawer, Crystal structure of a retroviral protease proves relationship to aspartic protease family, Nature 337 (1989) 576–579.
[4] M.A. Navia, P.M.D. Fitzgerald, B.M. McKeever, C.-T. Leu, J.C. Heimbach, W.K. Herber, I.S. Sigal, P.L. Darke, J.P. Springer, Three-dimensional structure of aspartyl protease from human immunodeficiency virus HIV-1, Nature 337 (1989) 615–620.
[5] N.D. Rawlings, A.J. Barrett, in: J.B. Alan (Ed.), Methods in Enzymology, Academic Press, 1995, pp. 105–120.
[6] B.M. Dunn, Structure, Mechanism of the pepsin-like family of aspartic peptidases, Chemical Reviews 102 (2002) 4431–4458.
[7] F. Grüninger-Leitch, D. Schlatter, E. Küng, P. Nelböck, H. Döbeli, Substrate and inhibitor profile of BACE (β-secretase) and comparison with other mammalian aspartic proteases, Journal of Biological Chemistry 277 (2002) 4687–4693.
[8] M.L. Hemming, J.E. Elias, S.P. Gygi, D.J. Selkoe, Identification of β-secretase (BACE1) substrates using quantitative proteomics, PLoS ONE 4 (2009) e8477.
[9] R. Vassar, B.D. Bennett, S. Babu-Khan, S. Kahn, E.A. Mendiaz, P. Denis, D.B. Teplow, S. Ross, P. Amarante, R. Loeloff, Y. Luo, S. Fisher, J. Fuller, S. Edenson, J. Lile, M.A. Jarosinski, A.L. Biere, E. Curran, T. Burgess, J.C. Louis, F. Collins, J. Treanor, G. Rogers, M. Citron, β-Secretase cleavage of Alzheimer's amyloid precursor protein by the transmembrane aspartic protease BACE, Science 286 (1999) 735–741.
[10] R. Yan, M.E. Bienkowski, M.E. Shuck, H. Miao, M.C. Tory, A.M. Pauley, J.R. Brashler, N.C. Stratman, W.R. Mathews, A.E. Buhl, D.B. Carter, A.G. Tomasselli, L.A. Parodi, R.L. Heinrikson, M.E. Gurney, Membrane-anchored aspartyl protease with Alzheimer's disease β-secretase activity, Nature 402 (1999) 533–537.
[11] T. Pillot, B. Drouet, S. Queille, C. Labeur, J. Vandekerckhove, M. Rosseneu, M. Pincon-Raymond, J. Chambaz, The nonfibrillar amyloid β-peptide induces apoptotic neuronal cell death. Involvement of its C-terminal fusogenic domain, Journal of Neurochemistry 73 (1999) 1626–1634.
[12] Z.M. Suo, J. Humphrey, A. Kundtz, F. Sethi, A. Placzek, F. Crawford, M. Mullan, Soluble Alzheimers β-amyloid constricts the cerebral vasculature in vivo, Neuroscience Letters 257 (1998) 77–80.
[13] J. Hardy, D.J. Selkoe, The amyloid hypothesis of Alzheimer's disease: progress and problems on the road to therapeutics, Science 297 (2002) 353–356.
[14] S. Sinha, J.P. Anderson, R. Barbour, G.S. Basi, R. Caccavello, D. Davis, M. Doan, H.F. Dovey, N. Frigon, J. Hong, K. Jacobson-Croak, N. Jewett, P. Keim, J. Knops, I. Lieberburg, M. Power, H. Tan, G. Tatsuno, J. Tung, D. Schenk, P. Seubert, S.M. Suomensaari, S. Wang, D. Walker, J. Zhao, L. McConlog, V. John, Purification and cloning of amyloid precursor protein β-secretase from human brain, Nature 402 (1999) 537–540.
[15] H. Cai, Y. Wang, D. McCarthy, H. Wen, D.R. Borchelt, D.L. Price, BACE1 is the major beta-secretase for generation of Aβ peptides by neurons, Nature Neuroscience 4 (2001) 233–234.
[16] Y. Luo, B. Bolon, S. Kahn, B.D. Bennett, S. Babu-Khan, P. Denis, W. Fan, H. Kha, J. Zhang, Y. Gong, L. Martin, J.-C. Louis, Q. Yan, W.G. Richards, M. Martin Citron, R. Vassar, Mice deficient in BACE1, the Alzheimer's β-secretase, have normal phenotype and abolished β-amyloid generation, Nature Neuroscience 4 (2001) 231–232.
[17] L. Hong, G. Koelsch, X. Lin, S. Wu, S. Terzyan, A.K. Ghosh, X.C. Zhang, J. Tang, Structure of the protease domain of memapsin 2 (b-secretase) complexed with inhibitor, Science 290 (2000) 150–153.
[18] L. Hong, R.T. Turner III, G. Koelsch, G. Shin, A.K. Ghosh, J. Tang, Crystal structure of memapsin 2 (β-secretase) complexed with an inhibitor OM00-3, Biochemistry 41 (2002) 10963–10967.
[19] L. Hong, J. Tang, Flap position of free memapsin 2 (β-secretase), a model for flap opening in aspartic protease catalysis, Biochemistry 43 (2004) 4689–4695.
[20] H. Shimizu, A. Tosaki, K. Kaneko, T. Hisano, T. Sakurai, N. Nukina, Crystal structure of an active form of BACE1, an enzyme responsible for amyloid β protein production, Molecular and Cellular Biology 28 (2008) 3663–3671.
[21] B. Xiong, X. Huang, L. Shen, J. Shen, X. Luo, X. Shen, H. Jiang, K. Chen, Conformational flexibility of β-secretase: molecular dynamics simulation and essential dynamics analysis, Acta Pharmacologica Sinica 25 (2004) 705–713.
[22] K. Suguna, E.A. Padlan, C.W. Smith, W.D. Carlson, D.R. Davies, Binding of a reduced peptide inhibitor to the aspartic proteinase from *Rhizopus chinensis*: implications for a mechanism of action, Proceedings of the National Academy of Sciences of the United States of America 84 (1987) 7009–7013.
[23] D. Chatfield, C.P. Eurenius, K. Brooks, R. Bernard, HIV-1 protease cleavage mechanism: a theoretical investigation based on classical MD simulation and reaction path calculations using a hybrid QM/MM potential, Journal of Molecular Structure: THEOCHEM 423 (1998) 79–92.
[24] S. Bjelic, J. Áqvist, Catalysis and linear free energy relationship in aspartic proteases, Biochemistry 45 (2006) 7709–7723.
[25] M. Cascella, C. Micheletti, U. Rothlisberger, P. Carloni, Evolutionarily conserved functional mechanics across pepsin-like and retroviral aspartic proteases, Journal of the American Chemical Society 127 (2005) 3734–3742.
[26] S. Piana, D. Bucher, P. Carloni, U. Rothlisberger, Reaction mechanism of HIV-1 protease by hybrid Car-Parrinello/Classical MD simulations, Journal of Physical Chemistry B 108 (2004) 11139–11149.
[27] J. Trylska, P. Grochowski, J.A. McCammon, The role of hydrogen bonding in the enzymatic reaction catalyzed by HIV-1 protease, Protein Science 13 (2004) 513–528.
[28] R. Singh, A. Barman, R. Prabhakar, Computational insights into aspartyl protease activity of presenilin 1 (PS1) generating Alzheimer amyloid β-peptides (Aβ40 and Aβ42), Journal of Physical Chemistry B 113 (2009) 2990–2999.
[29] A. Barman, S. Schürer, R. Prabhakar, Computational modeling of substrate specificity and catalysis of the β-secretase (BACE1) enzyme, Biochemistry 50 (2011) 4337–4349.
[30] I. Hussain, D. Powell, D.R. Howlett, D.G. Tew, T.D. Meek, C. Chapman, I.S. Gloger, K.E. Murphy, C.D. Southan, D.M. Ryan, T.S. Smith, D.L. Simmons, F.S. Walsh, C. Dingwall, G. Christie, Identification of a novel aspartic protease (Asp 2) as beta-secretase, Molecular and Cellular Neurosciences 14 (1999) 419–427.
[31] L. Coates, P.T. Erskine, S. Mall, R. Gill, S.P. Wood, D.A. Myles, J.B. Cooper, X-ray, neutron and NMR studies of the catalytic mechanism of aspartic proteinases, European Biophysics Journal 35 (2006) 559–566.
[32] L. Coates, H.-F. Tuan, S. Tomanicek, A. Kovalevsky, M. Mustyakimov, P.T. Erskine, J.B. Cooper, The catalytic mechanism of an aspartic proteinase explored with neutron and X-ray diffraction, Journal of the American Chemical Society 130 (2008) 7235–7237.
[33] R. Rajamani, C.H. Reynolds, Modeling the protonation states of the catalytic aspartates in β-secretase, Journal of Medicinal Chemistry 47 (2004) 5159–5166.
[34] X. Lin, G. Koelsch, S. Wu, D. Downs, A. Dashti, J. Tang, Human aspartic protease memapsin 2 cleaves the β-amyloid precursor protein, Proceedings of the National Academy of Sciences of the United States of America 97 (2000) 1456–1460.
[35] M. Strajbl, J. Florian, A. Warshel, Ab initio evaluation of the potential surface for general base-catalyzed methanolysis of formamide: a reference solution reaction for studies of serine proteases, Journal of the American Chemical Society 122 (2000) 5354–5366.
[36] Z. Wu, F. Ban, R.J. Boyd, Modeling the reaction mechanisms of the amide hydrolysis in an N-(o-carboxybenzoyl)-L-amino acid, Journal of the American Chemical Society 125 (2003) 6994–7000.
[37] H. Park, J. Suh, S. Lee, Ab initio studies on the catalytic mechanism of aspartic proteinases: nucleophilic versus general acid/general base mechanism, Journal of the American Chemical Society 122 (2000) 3901–3908.
[38] S. Piana, P. Carloni, M. Parrinello, Role of conformational fluctuations in the enzymatic reaction of HIV-1 protease, Journal of Molecular Biology 319 (2002) 567–583.
[39] A. Das, S. Mahale, V. Prashar, S. Bihani, J.L. Ferrer, M.V. Hosur, X-ray snapshot of HIV-1 protease in action: observation of tetrahedral intermediate and short ionic hydrogen bond SIHB with catalytic aspartate, Journal of the American Chemical Society 132 (2010) 6366–6373.
[40] M.J. Frisch, G.W. Trucks, H.B. Schlegel, G.E. Scuseria, M.A. Robb, J.R. Cheeseman, G. Scalmani, V. Barone, B. Mennucci, G.A. Petersson, H. Nakatsuji, M. Caricato, X. Li, H.P. Hratchian, A.F. Izmaylov, J. Bloino, G. Zheng, J.L. Sonnenberg, M. Hada, M. Ehara, K. Toyota, R. Fukuda, J. Hasegawa, M. Ishida, T. Nakajima, Y. Honda, O. Kitao, H. Nakai, T. Vreven, J. Montgomery, J.E. Peralta, F. Ogliaro, M. Bearpark, J.J. Heyd, E. Brothers, K.N. Kudin, V.N. Staroverov, R. Kobayashi, J. Normand, K. Raghavachari, A. Rendell, J.C. Burant, S.S. Iyengar, J. Tomasi, M. Cossi, N. Rega, N.J. Millam, M. Klene, J.E. Knox, J.B. Cross, V. Bakken, C. Adamo, J. Jaramillo, R. Gomperts, R.E. Stratmann, O. Yazyev, A.J. Austin, R. Cammi, C. Pomelli, J.W. Ochterski, R.L. Martin, K. Morokuma, V.G. Zakrzewski, G.A. Voth, P. Salvador, J.J. Dannenberg, S. Dapprich, A.D. Daniels, Ö. Farkas, J.B. Foresman, J.V. Ortiz, J. Cioslowski, D.J. Fox., Gaussian Inc., Wallingford, CT, 2009.
[41] T. Matsubara, S. Sieber, K. Morokuma, A test of the new integrated MO + MM (IMOMM) method for the conformational energy of ethane and n-butane, International Journal of Quantum Chemistry 60 (1996) 1101–1109.
[42] F. Maseras, K. Morokuma, IMOMM: a new integrated ab initio + molecular mechanics geometry optimization scheme of equilibrium structures and transition states, Journal of Computational Chemistry 16 (1995) 1170–1179.
[43] S. Humbel, S. Sieber, K. Morokuma, The IMOMO method: integration of different levels of molecular orbital approximations for geometry optimization of large systems: test for n-butane conformation and SN_2 reaction: $RCl + Cl^-$, Journal of Chemical Physics 105 (1996) 1959–1967.
[44] M. Svensson, S. Humbel, K. Morokuma, Energetics using the single point IMOMO (integrated molecular orbital + molecular orbital) calculations: choices of computational levels and model system, Journal of Chemical Physics 105 (1996) 3654–3661.
[45] S. Dapprich, I. Komáromi, K.S. Byun, K. Morokuma, M.J. Frisch, A new ONIOM implementation in Gaussian98. Part I. The calculation of energies, gradients, vibrational frequencies and electric field derivatives, Journal of Molecular Structure: THEOCHEM 461–462 (1999) 1–21.
[46] T. Vreven, K.S. Byun, I. Komáromi, S. Dapprich, J.A. Montgomery, K. Morokuma, M.J. Frisch, Combining quantum mechanics methods with molecular mechanics methods in ONIOM, Journal of Chemical Theory and Computation 2 (2006) 815–826.

[47] U.C. Singh, P.A. Kollman, A combined ab initio quantum mechanical and molecular mechanical method for carrying out simulations on complex molecular systems: applications to the $CH_3Cl + Cl^-$ exchange reaction and gas phase protonation of polyethers, Journal of Computational Chemistry 7 (1986) 718–730.
[48] M.J. Field, P.A. Bash, M. Karplus, A combined quantum mechanical and molecular mechanical potential for molecular dynamics simulations, Journal of Computational Chemistry 11 (1990) 700–733.
[49] A.D. Becke, Density-functional exchange-energy approximation with correct asymptotic behavior, Physical Review A 38 (1988) 3098.
[50] C. Lee, W. Yang, R.G. Parr, Development of the Colle-Salvetti correlation energy formula into a functional of the electron density, Physical Review B 37 (1988) 785–789.
[51] A.D. Becke, Density-functional thermochemistry. III. The role of exact exchange, Chemical Physics 98 (1993) 5648–5652.
[52] W.D. Cornell, P. Cieplak, C.I. Bayly, I.R. Gould, K.M. Merz, D.M. Ferguson, D.C. Spellmeyer, T. Fox, J.W. Caldwell, P.A. Kollman, A second generation force field for the simulation of proteins, nucleic acids, and organic molecules, Journal of the American Chemical Society 117 (1995) 5179–5197.
[53] M. Torrent, T. Vreven, D.G. Musaev, K. Morokuma, Ö. Farkas, H.B. Schlegel, Effects of the protein environment on the structure and energetics of active sites of metalloenzymes. ONIOM study of methane monooxygenase and ribonucleotide reductase, Journal of the American Chemical Society 124 (2001) 192–193.
[54] R.A. Kwiecien, I.V. Khavrutskii, D.G. Musaev, K. Morokuma, R. Banerjee, P. Paneth, Computational insights into the mechanism of radical generation in B12-dependent methylmalonyl-CoA mutase, Journal of the American Chemical Society 128 (2006) 1287–1292.
[55] J. Alí-Torres, J.-D. Mareïchal, L. Rodríguez-Santiago, M. Sodupe, Three dimensional models of Cu_2^+-Aβ(1–16) complexes from computational approaches, Journal of the American Chemical Society 133 (2011) 15008–15014.
[56] E.F. Oliveira, N.M.F.S.A. Cerqueira, P.A. Fernandes, M.J. Ramos, Mechanism of formation of the internal aldimine in pyridoxal 5′-phosphate-dependent enzymes, Journal of the American Chemical Society 133 (2011) 15496–15505.
[57] L.R. Rutledge, S.D. Wetmore, Modeling the chemical step utilized by human alkyladenine DNA glycosylase: a concerted mechanism aids in selectively excising damaged purines, Journal of the American Chemical Society 133 (2011) 16258–16269.
[58] C. Greco, M. Bruschi, P. Fantucci, U. Ryde, L. De Gioia, Mechanistic and physiological implications of the interplay among iron–sulfur clusters in [FeFe]-hydrogenases. A QM/MM perspective, Journal of the American Chemical Society 133 (2011) 18742–18749.
[59] M. Lundberg, K. Morokuma, Protein environment facilitates O2 binding in nonheme iron enzyme. An insight from ONIOM calculations on isopenicillin N synthase (IPNS), Journal of Physical Chemistry B 111 (2007) 9380–9389.
[60] R. Prabhakar, T. Vreven, M.J. Frisch, K. Morokuma, D.G. Musaev, Is the protein surrounding the active site critical for hydrogen peroxide reduction by selenoprotein glutathione peroxidase? An ONIOM study, Journal of Physical Chemistry B 110 (2006) 13608–13613.
[61] V. Carnevale, S. Raugei, S. Piana, P. Carloni, On the nature of the reaction intermediate in the HIV-1 protease: a quantum chemical study, Computer Physics Communications 179 (2008) 120–123.
[62] L. Zheng, M. Chen, W. Yang, Random walk in orthogonal space to achieve efficient free-energy simulation of complex systems, Proceedings of the National Academy of Sciences of the United States of America 105 (2008) 20227–20232.